IDEASSat: A 3U CubeSat mission next on the pad for ionospheric science

Y. Duann, L. C. Chang, C. -K. Chao, Y. -C. Chiu, C. C. J. H. Salinas,

R. Tsai-Lin, T. -Y. Tai, W. -H. Luo, C. -T. Liao, H. -T. Liu,

C. -J. Chung, J. -Y. Liu, G. F. Gacal, S. Denduonghatai

Center for Astronautical Physics and Engineering, Institute of Space Science and Engineering,

National Central University, Taiwan

A. Chandran

Laboratory for Atmospheric and Space Physics,

University of Colorado at Boulder, Boulder, CO, USA;

Satellite Research Centre,

Nanyang Technological University, Singapore

H. Priyardarshan, Ankit Verma

Department of Avionics,

Indian Institute of Space Science and Technology, Kerala, India

T. -W. Fang

CIRES/University of Colorado at Boulder,

Boulder, CO, USA;

Satellite Research Centre,

Nanyang Technological University, Singapore

S. Srivastava

Satellite Research Centre,

Nanyang Technological University, Singapore

Abstract

Following the growing use of small satellites as a platform for distributed aeronomy observations, the Ionospheric Dynamics Exploration and Attitude Subsystem Satellite (IDEASSat/INSPIRESat-2) is a three-unit (U) CubeSat that has been developed by National Central University (NCU) in partnership with the International Satellite Program in Research and Education (INSPIRE) consortium, and funded by the Taiwan National Space Organization (NSPO), Ministry of Science and Technology, and Ministry of Education as part of the first national effort to encourage small satellite development at Taiwan universities. IDEASSat is scheduled to be launched into a 500 km Sun-synchronous orbit (SSO, 97.41° inclination) in December 2020, and the data are scheduled to be released online for global user 2 to 6 months after launch. The objective of IDEASSat mission is to provide in-situ measurements of the Earth's ionosphere in order to quantify both global scale ionospheric variability and small-scale irregularities. The science payload is the Compact Ionospheric Probe (CIP, ~0.4 kg) - an all in one in-situ plasma sensor developed at Taiwan National Central University (NCU), which is the miniaturized version of the larger Advanced Ionospheric

Probe (AIP, ~4.5 kg) that is carried and operational aboard the 450 kg FORMOSAT-5 spacecraft. Oriented in the ram direction, CIP provides raw data of ion and electron currents from which ion and electron temperature, ion density, ion drift velocity, and light to heavy ion ratio can be derived with sampling rates of up to 8 Hz. With high sampling rate and pointing accuracy, IDEASSat CIP can provide snapshots of the spatial structure of plasma irregularities and the traveling ionospheric disturbances (TIDs) with sub-kilometer resolution in Low Earth Orbit. The development of IDEASSat has not only offered students a hands-on opportunity to learn about space science and technology, but also works in conjunction with CIPs carried onboard the INSPIRESat-1, ARCADE/INSPIRESat-4, and SCION-X/INSPIRESat-6 small satellites, as well as the AIP carried by FORMOSAT-5. This allows for multi-platform observations spanning different altitudes and local times, to improve our understanding of the ionosphere. This presentation will focus on the potential space phenomena that the IDEASSat observe, and the global pattern that INSPIRE constellation can outline with FORMOSAT-5 AIP measurements.

Key word: INSPIRE, cubesat, Compact Ionospheric Probe, constellation, ionospheric science

1. Introduction

The International Satellite Program in Research and Education (INSPIRE) consortium was formed in 2015, initially comprised of the University of Colorado at Boulder (CU), National Central University in Taiwan (NCU), and the Indian Institute of Space Science and Technology (IIST). The INSPIRE consortium has expanded to 11 institutions as of 2020, with six small satellite science missions funded from sources secured by the participating institutions (*Baker and Chandran*, 2018; *Chang et al.*, 2018b). The Earth's upper atmosphere have been focused as studying regime by a large number of satellite missions, including the neutral thermosphere (90 – above 500 km altitude) and mesosphere (60 – 90 km), as well as the ionosphere (60 – 1000 km). The neutral particles are ionized in the photochemical process by different wavelengths of solar emission, and form the ionized part of the upper atmosphere, which is the ionosphere. The phenomena of strong day-night difference as well as latitudinal, seasonal, and solar cycle variability are the mainstream research to understand the ionosphere. The radio scintillations and signal fading at receiver end occur when the signals pass through the irregularities of plasma in the ionosphere such as plasma bubbles and Travelling Ionospheric Disturbances (TIDs), as a consequence of random fluctuations of the refraction index (*Zhong et al.*, 2008). The changes in the ionosphere have significant effect on radio propagation and Global Navigation Satellite System (GNSS) signals (*Frissell et al.*, 2014), as well as the electric charging of spacecraft orbiting through the ionosphere.

This conference paper is focusing on the scientific objectives of the Ionospheric Dynamics Exploration and Attitude Subsystem Satellite (IDEASSat/INSPIRESat-2, hereafter referred to as IDEASSat). Measurement of ionospheric plasma parameters at planetary scales, with high resolution sampling rate to resolve the small scales irregularities, the global coverage of IDEASSat with the constellation included of INSPIRESat-1, ARCADE/INSPIRESat-4, and SCION-X/INSPIRESat-6 small satellites, as well as the Advanced Ionospheric Probe (AIP) carried by FORMOSAT-5 in different orbit planes, are designed for studying planetary-scale wave structures in the ionosphere, the distribution of ionospheric irregularities and Travelling Ionospheric Disturbances (TIDs), as well as the electric fields driving vertical plasma drifts, and their relation to the ionospheric F region wind dynamo (*Duann et al.*, 2020).

2. Mission overview

The IDEASSat 3U CubeSat mission development began as one of the missions in the International Satellite Program in Research and Education (INSPIRE) consortium in May 2017 (*Chang et al.*, 2018a), and funded by the Taiwan National Space Organization (NSPO), Ministry of Science and Technology, and Ministry of Education. The primary objectives of IDEASSat mission are listed in the Science Traceability Matrix (Table 1). (1) Measuring planetary-scale wave structures in the ionosphere, and quantifying their variability and contribution to ionospheric morphology; (2) Measuring the distribution, and structure of ionospheric irregularities and Travelling Ionospheric Disturbances (TIDs); (3) Inferring the electric fields driving vertical plasma drifts, and their relation to the ionospheric F region wind dynamo. A secondary mission involving the capture of star tracker images for attitude determination algorithm tests will be performed (*Duann et al.*, 2020).

The IDEASSat flight model (FM) is scheduled to be launched into a 500 km Sun-synchronous orbit (SSO, 97.41° inclination) with a local time of descending node (LTDN) between 10:00 and 12:00 in December 2020, and the data are scheduled to be released online for global user 2 to 6 months after launch. The LTDN of IDEASSat is close to the 720 km orbital plane of the FORMOSAT-5 carrying AIP with LTDN at 10:30, allowing for observations at different altitudes within this local time sector. The INSPIRESat-1 and SCION-X/INSPIRESat-6 are scheduled to be launched into ~500 km altitude circular orbit with different inclination and LTDN, and ARCADE/INSPIRESat-4 will be orbiting at ~535 km altitude for the first 6 months, and lower the orbit to ~300 km altitude. Once at 300 km, ARCADE prograde thruster operation will be used to prevent rapid decay of the orbit. The AIP is an all in one in-situ plasma sensor containing

Table 1. IDEASSat Secondary Science Traceability Matrix

Science Traceability Matrix		
Science Objectives	**Objectives Measurement**	**Measurement Requirements (Capabilities)**
S1. To measure planetary- scale wave structures in the ionosphere, and quantify their variability and contribution to ionospheric morphology. **S2.** To measure the distribution, occurrence rate, and structure of ionospheric irregularities and Travelling Ionospheric Disturbances (TIDs). **S3.** To infer the electric fields driving vertical plasma drifts, and their relation to the ionospheric F region wind dynamo.	Ionospheric parameters in the F-region (400 ~ 600 km altitude). 20 km (100 km) horizontal sampling resolution. Latitude range exceeding $\pm 30°$. 400 ~ 600 km orbital plane in quadrature or parallel with DMSP/ FORMOSAT-5. Likely 0930 ~ 1030. Observations for at least six months.	Horizontal resolution: At least 0.5x the horizontal scale of a typical plasma bubble. Orbit: Pointing knowledge (<0.1°). Pointing stability (<0.5°). Lifetime: 6 months.
Instrumentation	**Instrument Requirements (Capabilities)**	**Data Processing Requirements (Capabilities)**
Compact Ionosphere Probe (CIP)	90° FOV. Power: <5 W Pointing Accuracy: Ram pointing, $< 0.5°$ Pointing Knowledge: $< 0.1°$ Science Data Packet Size: 280 bytes/ packet	Onboard Storage (1 month of data): >5 GB Daily Downlink: 24.8 MB/day, 1 raw data packet per second, full mode cycle per 3 s (4.6 MB/day, if sampled as 1 raw data packet per 15 s).
E1. To collect Star tracker images from Attitude Determination and Control Subsystem (ADCS).	Spacecraft attitude and angular velocities. Spacecraft position and time. Star tracker imagery.	Operation during eclipse. Campaign to be performed when scheduling and power requirements allow.
Instrumentation	**Instrument Requirements (Capabilities)**	**Data Processing Requirements (Capabilities)**
GPS Blue Canyon Technologies (BCT) XACT ADCS module	Image Size: 2.811 MB Volume: 1U. Mass: 500 g. Chassis Aperture: 25 mm. FOV: 7°.	Attitude Determination Experiment: Daily Downlink: 12.05 MB/day

Retarding Potential Analyzer (RPA), Ion Drift Meters (IDM), Planar Langmuir Probe (PLP), and Ion Trap (IT) operating modes with a current reading rate of up to 8,192 Hz, to measure the ion concentration, ion temperature, ram velocity, and arrival angle of the incoming ions. The data package sampling rate varies for different operating modes. In the nominal mode it is 1 package (1,024 bytes) per 3 seconds, the fast mode sampling rate is 8 times that of nominal mode, and the burst mode is 64 times that of nominal mode. At the time of launch, AIP was one of the lightest and fastest sampling rate payloads to perform in-situ measurement of ionosphere physical parameters (*Lin et al.*, 2017). The CIP (~0.4 kg) is a minimized version of the AIP (~4.5 kg), with the smaller volume and less mass, the CIP is designed for the purpose of in-situ measuring plasma parameters onboard CubeSat missions.

3. Scientific objectives

This section provides the relation of scientific objectives and IDEASSat mission design, and how IDEASSat serves to complement and extends the ionospheric observation missions over the past 20 years, such as FORMOSAT-1, the Challenging Minisatellite Payload (CHAMP), the Defense Meteorological Satellite Program (DMSP) F-16 spacecraft, the Detection of Electromagnetic Emissions Transmitted from Earthquake Regions (DEMETER), the Communications/Navigation Outage Forecasting System (C/NOFS) and FORMOSAT-5 (*Yeh et al.*, 1999; *Reigber et al.*, 1999; *Le et al.*, 2003; *Gwal et al.*, 2005; *Rodrigues et al.*, 2009; *Lin et al.*, 2017). The usage of in-situ instruments for measuring ionosphere, can prevent the inaccuracy caused by complex calibration

of large distance and angle projections inherent in remote sensing missions, decreases measurement uncertainties and results in higher resolution (*Teillet et al.*, 2003). In-situ instruments sample along the spacecraft orbit. The in-situ sensors form the electric potentials as I-V curve, and a complete I-V curve is required in order to derive specific ionospheric plasma parameters, such as ion and electron density and temperature (*Merlino*, 2007).

3.1 Plasma irregularities and Traveling Ionospheric Disturbances

Severe scintillation resulted from the small-scale irregularities in the ionosphere can render satellite communications and global navigation satellite systems (GNSS) unusable (*Kelly et al.*, 2014). The small-scale plasma irregularities are associated with the density enhancement and depletion. The plasma bubbles and plumes are localized plasma density depletion in the ionosphere, and are usually the consequence of the Rayleigh-Taylor (R-T) instability in the *F*-region of ionosphere (*Dungey*, 1956). R-T instability began the development with the opposite direction of density gradient and gravity force in the ionosphere. This phenomenon usually occurs at the dusk terminator, when the ions subside downward and increase the ionized density at lower altitude, speed up the recombination rate, and reduce the ionized density rapidly by recombining ionized particles into neutral particles. While the top side of the ionosphere is still in sunlit, photochemical process remains a relatively stable condition to maintain the ionized density, and the ionized density gradient therefore becomes vertically upward. The net current flows $\vec{\mathrm{J}}$ is in the direction of $\vec{\mathrm{g}} \times \vec{\mathrm{B}}$, which is strictly horizontal, and accumulates more and more ionized particles at the boundary of the perturbation. The perturbed $\delta\vec{E}$ builds up, and the irregularities are developed by rising or dropping the portions of plasma with the $\delta\vec{E} \times \vec{\mathrm{B}}$ drift (*Kelly*, 2009).

The plasma density depletion extending beyond the ionospheric peak in the region of strong equatorial spread F (ESF, spread of echoes over a range of virtual heights, or over a range of frequency for a given virtual height) is first reported by the observation of incoherent scatter (IS) radar at the equatorial station Jicamarca. It is suggested that the bubble-like structures, which has lower density inside the structure itself than that of the surroundings, rise by the effect of buoyancy and continue the motion even in the topside regions of the ionosphere along the geomagnetic field lines covering up to $\pm 30°$ magnetic latitude in the extreme cases, sometimes over 700 km height (*Woodman and La Hoz*, 1976). Pre-reversal enhancement (PRE) is an enhancement of the vertical $\vec{E} \times \vec{\mathrm{B}}$ drift due to the eastward electric field at the magnetic equator dusk terminator, and PRE is believed to be one of the dominant factor for the generation of equatorial plasma bubbles (EPBs) (*Abdu*, 2001). There have been many ground-based and satellite-based observations, that have shown the connection between PRE and EPBs (*Abadi et al.*, 2015; *Dabas et al.*, 2003; *Huang and Hairston*, 2015; *Tulasi Ram et al.*, 2006). The equatorial ionospheric anomaly (EIA) is observed and defined as a large structure with a trough near equator, crests near ±15° magnetic latitudes and crest-to-trough ratio ~1.6 in daytime peak electron density (*Namba and Maeda*, 1939; *Appleton*, 1946). EIA begins to develop in the morning around 10 LT, and continues to exist well even beyond sunset, the formation of EIA is suggested to be associated with the equatorial plasma fountain (EPF) (*Martyn*, 1955; *Rishbeth et al.*, 1963). During PRE of the upward $\vec{E} \times \vec{\mathrm{B}}$ drift and reverse plasma fountain during the following downward drift, the fountain is impulsively strengthened. The mechanisms controlling the daily variation of PRE still have not been investigated well yet (*Ghosh et al.*, 2020). The EPB could rise in height by 200 km in 7.8 min with the vertical growth rate ~427 m/s, is shown in the 3-dimensional simulation of plasma plumes by *Retterer* (2010), this result indicates that the observation is required to be high measurement sampling rate. A single satellite passing through a plasma bubble will garner a 1-D spatial perspective of the bubbles shape and size at some instant in time.

The close relationship between EPBs and the medium-scale traveling ionospheric disturbances (MSTIDs) over South American Equatorial regions in July 2014 were observed by *Takahashi et al.* (2018). The traveling ionospheric disturbances (TIDs) are identified as propagating perturbations in the ionospheric electron density (*Fedorenko et al.*, 2013), and usually classified into two classes based on velocity and wavelength: medium-scale (MS) and large-scale (LS) waves, the classification is shown in Table 2 (*Hocke and Schlegel*, 1996). The phase speed of LSTIDs is approximately 700 m/s (*Pradipta et al.*, 2016), while the phase speed of MSTID is around 100–300 m/s (*Hunsucker*, 1982). The horizontal velocity of the MSTIDs is less than 0.25 km/s and that of the LSTID is 0.4–1000 km/s.

Table 2. The parameters of MSTID and LSTID.

	MSTID	LSTID
Wavelength (km)	100 – 600	>1000
Temporal Period (hr)	0.25 – 1	0.5 – 4
Horizontal Velocity (km/s)	<0.25	0.4 – 1000
Phase Speed (m/s)	100 – 300	~700

There are two groups of MSTIDs classified by the different causes: (1) The MSTIDs generated via electrodynamical forces under the condition of the Perkins instability (*Perkins*, 1973). (2) The MSTIDs generated via atmospheric gravity waves (AGWs) propagating in the F-layer bottom side (*Otsuka et al.*, 2013). However, the conditions and types of MSTIDs that are effective in generating EPBs are still unknown. To study the TID and the relation of it and EPBs, the spacecraft is required to be able to measure the ion velocities cross track and in the ram direction within a range of ± 2.5 km/s (cross track) and -7.5 ± 1 km/s (ram) at a sensitivity of ± 10 m/s (cross track) and ± 100 m/s (ram), with an accuracy of

± 50 m/s (cross track) and ± 200 m/s (ram). Relative to the CIP oriented in the ram direction, ion velocity is detected when the ions move into the IT, and hence the baseline is negative. The IDEASSat CIP will be able to provide a snapshot of the spatial structure of these irregularities, with the high value of the spacecraft velocity and high measurement sampling rate (*Duann et al.*, 2020).

3.2 Ionospheric planetary scale structure

Planetary-scale structures are defined as having wavelengths that are harmonics of the Earth's circumference. Such structure can be generated by photoionization, as well as vertical coupling from atmospheric tides and planetary waves (PWs) that propagate into the ionosphere from below (*Chang et al.*, 2013a; *Chang et al.*, 2013b; *Chang et al.*, 2014). The vertical plasma drifts of the equatorial fountain formed by the wind dynamo mechanism can be modulated by the PWs and atmospheric tides capable of propagating into the ionospheric *E* region. The periodicities and zonal wavenumbers of these PWs and atmospheric tides can be reflected in the ionospheric *F* region above. The effects of the *E*-region dynamo combined with transport effects in the *F* region is related to the wave-4 structure observed at high altitudes in ionosphere (*Onohara et al.*, 2018), which is defined as the four-peaked longitudinal structure that is a persistent feature of the low-latitude ionosphere system (*Immel et al.*, 2006; *Chang et al.*, 2010).

The global scale observations of IDEASSat combine with multi-platform INSPIRESats and FORMOSat-5/AIP observations will allow for the identification of such planetary-scale structures in the low latitude ionosphere.

4. Science Payload: Compact Ionospheric Probe (CIP)

The payload for IDEASSat is the NCU-developed Compact Ionospheric Probe (CIP) - an in-situ plasma sensor that meets the ionospheric Science objectives of IDEASSat (Table 1). To function within a 3U CubeSat, CIP is a miniaturized of AIP, the mass of CIP is 0.4 kg, with a volume of about 0.8U. Both contain the sensors of Planar Langmuir Probe (PLP) to measure electron temperature; Ion Trap (IT) to measure ion density; Retarding Potential Analyzer (RPA) to measure light/ heavy ion mass ratio, ion temperature, and ion ram speed; and Ion Drift Meter (IDM) to detect ion arrival angles.

The mechanical structure of CIP within the whole spacecraft is shown in Fig. 1. The Aperture and Meshes Module (AMM) is the golden assembly on the top of CIP, exposing to the plasma environment during the measurement. The stacking green boards are Analog Preprocessing Unit (APU), Digital Control Unit (DCU), and Power Management Unit (PMU), respectively.

CIP typically cycles through three measurement modes every 3 s (PLP-RPAIDM) in both Normal and Fast mode, returning 3 data packets in Normal mode, or 24

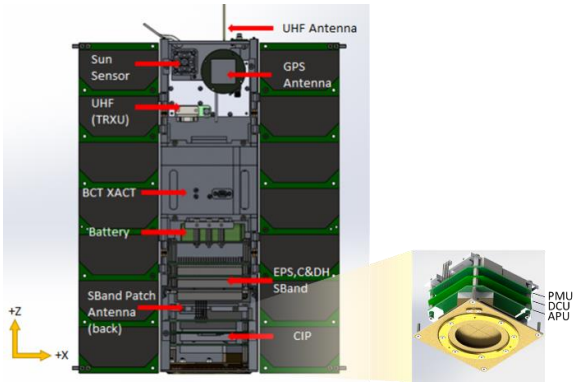

Figure 1. The structures of IDEASSat (left) and CIP (right). The body mounted solar panel on the -y face is not shown, in order to elucidate the spacecraft interior. For CIP, APU is Analog Preprocessing Unit, DCU is Digital Control Unit, and PMU is Power Management Unit (*Duann et al.*, 2020).

packets in Fast mode, from which the ionospheric parameters can be derived. With sampling rate of up to 8 Hz, science data allows for horizontal resolution of ionospheric features with scales on the order of 1 km, thereby satisfying the mission objective with respect to ionospheric irregularities mentioned in previous section. CIP only operates when the spacecraft is in eclipse, while during the Fast mode, with 40% CIP duty cycle per orbit, the data generation per day is 212.90 MB. The science data packets contain the following parameters: universal time (UT), spacecraft position, spacecraft velocity, and spacecraft attitude knowledge such as roll angle, pitch angle, and yaw angle in LVLH (Local Vertical Local Horizon) coordinate (*Duann et al.*, 2020).

5. Spacecraft

The structure of IDEASSat 3U CubeSat is mainly composed of aluminum (AL 6061-T6), and it meets the CalPoly CubeSat Design Specifications of 0.9 mm and 4.5 kg (*Mehrparvar et al.*, 2014). The INSPIRE team at NCU and IIST developed the Command and Data Handling Subsystem (C&DH) and Electric Power Subsystem (EPS), and the deployable Ultra high frequency (UHF) tape measure antenna is also made inhouse based on the Miniature X-ray Solar Spectrometer (MinXSS) CubeSat heritage design (*Woods et al.*, 2013). Power requirements are satisfied with 4 Lithium ion batteries and 20 AzurSpace TJ 3G30A solar cells, ADCS and communications subsystems are utilized with commercial off the shelf (COTS). The fine pointing requirements of CIP are satisfied with a Blue Canyon Technologies (BCT) XACT ADCS with Global Positioning System (GPS) receiver (*Mason et al.*, 2018). The SpaceQuest (SQ) TRX-U transceiver is used for UHF communications on the spacecraft end, in conjunction with a monopole tape measure antenna for beaconing and receiving commands from the ground station end, and the UHF telemetry of IDEASSat uses 9600 bits per second (bps) GMSK modulation with the AX.25 data link protocol. For the S-

band transmitter, the Clyde Space STXC transmitter developed by Cape Peninsula University of Technology (CPUT) is selected, which also satisfies related data downlink requirements. This band is allocated by both the Taiwan NCC and ITU Region 3 to space research, space operation, and Earth exploration satellites (*Ministry of Transportation and Communications*, 2017). The S-Band rate is modified as 1 Megabits per second (Mbps) for the best communicating condition. Each access times to the ground stations are only considered for data downlink if they are longer than 5 min, combining the Boulder, Taiwan, Singapore S-band ground stations, this is sufficient to downlink the expected CIP science data produced. Thermal analysis of the spacecraft on the component level was performed using Thermal Desktop to simulate the expected spacecraft temperatures under worst case cold (Phoenix mode eclipse), worst case hot (Charging mode sunlight) conditions, as well as Nominal operations. Passive control mechanisms keep all components are within an operational temperature range as the result of thermal analysis simulated by using Thermal Desktop. The IDEASSat FM is undergoing the phase of testings.

As shown in the Fig. 1, the spacecraft coordinate system is defined with the CIP aperture pointing in the -Z direction, and the normal of the deployed and body mounted solar panels pointing in the -Y direction. The UHF tape measure antenna is deployed in the +Z direction. S-Band and GPS patch antennas are respectively attached to the -Y and +Y sides of IDEASSat. In a deployed state, the deployable and body mounted solar panels, as well as a coarse Sun sensor are located on the -Y side of the spacecraft.

6. Conclusions

The IDEASSat 3U CubeSat carrying scientific payload CIP, is designed to study the ionospheric variability, including structures on planetary scales and smaller scales on the order of 1 km. In this manuscript, we focus on the scientific objectives and the design of IDEASSat for the purpose of capturing the phenomena of interest. This mission has benefited greatly through international collaboration via the INSPIRE consortium, and has served as a useful capacity building exercise for spacecraft engineering at NCU. IDEASSat is scheduled to be launched into a 500 km Sun-synchronous orbit (SSO, 97.41° inclination) in December 2020, and the data are scheduled to be released online to benefit global users 2 to 6 months after launch. As one of the missions in INSPIRE consortium, IDEASSat will greatly expand observational capability for in-situ ionospheric measurements.

Reference

Abadi, P., Y. Otsuka, T. Tsugawa (2015), Effects of pre-reversal enhancement of E × B drift on the latitudinal extension of plasma bubble in southeast asia international CAWSES-II symposium, Earth Planets Space, doi:10.1186/s40623-015-0246-7.

Abdu M. A. (2001), Outstanding problems in the equatorial ionosphere-thermosphere electrodynamics relevant to spread F, J. Atmos. Solar-Terrestrial Phys., 63, 869–884, doi:10.1016/S1364-6826(00)00201-7.

Appleton, E. V. (1946), Two anomalies in the ionosphere. Nature, 157(3995), 691, doi:10.1038/157691a0.

Baker, D. N., A. Chandran (2018), Space, still the final frontier, Science. 361(207), Iss. 6399, pp. 207, doi: 10.1126/science.aau7631.

Chang, L. C., S. E. Palo, H. -L. Liu, T. -W. Fang, C. S. Lin (2010), Response of the thermosphere and ionosphere to an ultra fast Kelvin wave., J. Geophys. Res., 115, A00G04, doi:10.1029/2010JA015453.

Chang, L. C., C. -K. Chao, C. -L. Kuo, J. -Y. Liu, Y. Duann, A. Chandran, T. -W. Fang, H. Priyadarshan, A. K. Kaustubh, W. Evonosky (2018a), IDEASSat: the ionosphere dynamics explorer and attitude subsystem satellite, In: SSC18-WKIV-06, Proceedings of the 32nd Annual AIAA/USU Conference on Small Satellites, Logan, UT, USA.

Chang, L. C., C. K. Chao, A. Chandran, C.-L. Kuo, J. -Y. Liu, Y. Duann, Y. -C. Chiu, R. Tsai-Lin, W. -H. Luo, T. -Y. Tai, C. -T. Liao, H. -T. Liu, C. -J. Chung, R. Duann, Z. -M. Yang (2018b), IDEASSat – A 3U CubeSat for ionospheric science and capacity building. In: IAC-18-B4.2.6, 69th International Astronautical Congress (IAC), Bremen, Germany, 1–5 October 2018.

Dabas, R. S., L. Singh, D. R. Lakshmi, P. Subramanyam, P. Chopra, S. C. Garg (2003), Evolution and dynamics of equatorial plasma bubbles: relationships to ExB drift, postsunset total electron content enhancements, and equatorial electrojet strength, Radio Sci 38(4):1075, doi:10.1029/2001RS002586.

Duann, Y., L. C. Chang, C. -K. Chao, Y. -C. Chiu, R. Tsai-Lin, T. -Y. Tai, W. -H. Luo, C. -T. Liao, H. -T. Liu, C. -J. Chung, R. Duann, C. -L. Kuo, J. -Y. Liu, Z. -M. Yang, G. F. Gacal, A. Chandran, H. Priyardarshan, A. Verma, T. -W. Fang, S. Srivastav (2020), IDEASSat: A 3U CubeSat mission for ionospheric science, Adv. in Space Res., 66(1), 116-134, doi:10.1016/j.asr.2020.01.012.

Dungey, J. W. (1956), Convective diffusion in the equatorial F-region, J. Atmos. Terr. Phys., 9, 304.

Fedorenko, Y. P., O. F. Tyrnov, V. N. Fedorenko, V. L. Dorohov (2013), Model of traveling ionospheric disturbances, J. Space Weather Space Clim., 3 (A30), doi:10.1051/swsc/2013052.

Frissell, N. A., E. S. Miller, S. R. Kaeppler, F. Ceglia, D. Pascoe, N. Sinanis, P. Smith, R. Williams, A. Shovkoplyas (2014), Ionospheric sounding using real-time amateur radio reporting networks, Space Weather, 12, 651–656, doi:10.1002/2014SW001132.

Ghosh, P., Y. Otsuka, S. Mani (2020), Day-to-day variation of pre-reversal enhancement in the equatorial ionosphere based on GAIA model simulations, Earth Planets Space 72, 93, doi:0.1186/s40623-020-01228-9.

Gwal, A. K., M. Parrot, J. L. Pincon, J. P. Lebreton, A. Trigunait, S. Sarkar, K. Malhotra, N. Sharma (2005), Variation of electron density above india observed by DEMETER microsatellite and the CRABEX project, In: Proceedings of the XXVIIIth URSI General Assembly, October 2005, New Delhi, India.

Huang, C., M. R. Hairston (2015), The postsunset vertical plasma drift and its effects on the generation of equatorial plasma bubbles observed by the C/NOFS satellite, J. Geophys. Res. Space Phys., 120, 2263–2275, doi:10.1002/2014JA020735.

Hunsucker, R. D. (1982), Atmospheric gravity waves generated in the high latitude ionosphere: a review, Rev. Geophys., 20(2), 293-315. ISSN: 1944-9208, 1, 5, 127, 129.

Immel, T. J., E. Sagawa, S. L. England, S. B. Henderson, M. E. Hagan, S. B. Mende, H. U. Frey, C. M. Swenson, L. J. Paxton (2006), Control of equatorial ionospheric morphology by atmospheric tides, Geophys. Res. Lett., 33 (15), doi:10.1029/2006GL026161.

Kelly, M. C. (2009), The Earth's ionosphere: plasma physics and electrodynamics (International Geophysics Series), Second edition, Academic, San Diego, CA USA, 43, 142 – 148, ISBN: 978-0-12-088425-4.

Kelly, M. A., J. M. Comberiate, E. S. Miller, L. J. Paxton (2014), Progress toward forecasting of space weather effects on UHF SATCOM after Operation Anaconda, Space Weather, 12, 601–611, doi:10.1002/2014SW001081.

Le, G., C. -S. Huang, R. F. Pfaff, S. -Y. Su, H. -C. Yeh, R. A. Heelis, F. J. Rich, M. Hairston (2003), Plasma density enhancements associated with equatorial spread F: ROCSAT-1 and DMSP observations, J. Geophys. Res., 108 (A8), 1318, doi:10.1029/2002JA009592.

Lin, Z. W., C. K. Chao, J. Y. Liu, C. M. Huang, Y. H. Chu, C. L. Su, Y. C. Mao, Y. S. Chang (2017), Advanced Ionospheric Probe scientific mission onboard FORMOSAT-5 satellite, Terr. Atmos. Ocean. Sci., 28, 99–110, doi:10.3319/TAO.2016.09.14.01(EOF5).

Martyn, D. F. (1955), Theory of height and ionization density changes at the maximum of a Chapman-like region, taking account of ion production, decay, diffusion, and total drift, In: Proceedings, Cambridge Conference, London: Physical Society, 254.

Mason, J. P., B. Lamprecht, C. Downs, T. N. Woods (2018), CubeSat onorbit temperature comparison to thermal-balance-tuned model predictions, J. Thermophys. Heat Transf., 32 (1), 237–255, doi:10.2514/1.T5169.

Merlino, R. L. (2007), Understanding Langmuir probe current-voltage characteristics, Am. J. Phys., 75 (12), 1078–1085, doi:10.1119/1.2772282.

Mehrparvar, A., D. Pignatelli, J. Carnahan, R. Munakata, W. Lan, A. Toorian, A. Hutputanasin, S. Lee (2014), CubeSat Design Specification, Rev., 13, The CubeSat Program, Cal Poly SLO.

Ministry of Transportation and Communications (2017), Table of Radio Frequency Allocations of the Republic of China, 2017.2 Revised, retrieved from: https://freqdbo.ncc.gov.tw/Portal/NCCB03F_.aspx.

Namba, S., and K. -I. Maeda (1939), Radio Wave Propagation, 86, Corona, Tokyo.

Onohara, A. N., I. S. Batista, P. P. Batista (2018), Wavenumber-4 structures observed in the low-latitude ionosphere during low and high solar activity periods using FORMOSAT/COSMIC observations, Ann. Geophys., 36, 459–471, doi:10.5194/angeo-36-459-2018.

Otsuka, Y., K. Suzuki, S. Nakagawa, M. Nishioka, K. Shiokawa, T. Tsugawa (2013), GPS observations of medium-scale traveling ionospheric disturbances over Europe, Ann. Geophys., 31, 163–172, doi:10.5194/angeo-31-163-2013.

Perkins, F. (1973), Spread F and ionospheric currents, J. Geophys. Res., 78(1), 218–226, doi:10.1029/JA078i001p00218.

Pradipta, R., C. E. Valladares, B. A. Carter, P. H. Doherty (2016), Interhemispheric propagation and interactions of auroral traveling ionospheric disturbances near the equator, J. Geophys. Res. Space Phys., 121, 2462–2474, doi:10.1002/2015JA022043.

Priyadarshi, S. (2015), A Review of Ionospheric Scintillation Models, Surv. Geophys., 36, 295–324, doi:10.1007/s10712-015-9319-1.

Reigber, Ch., P. Schwintzer, H. Lühr (1999), The CHAMP geopotential mission, in Bollettino di

Geofisica Teorica ed Applicata, 40(3–4), 285–289, ISSN: 0006-6729.

Retterer, J.M., (2010), Forecasting low-latitude radio scintillation with 3-D ionospheric plume models: 1. Plume model, J. Geophys. Res., 115, A03306, doi:10.1029/2008JA013839.

Rishbeth, H., A. J. Lyon, and M. Peart (1963), Diffusion in the equatorial F layer, J. Geophys. Res., 68(9), 2559–2569, doi:10.1029/JZ068i009p02559

Rodrigues, F. S., M. C. Kelley, P. A. Roddy, D. E. Hunton, R. F. Pfaff, O. de La Beaujardiere, G. S. Bust (2009), C/NOFS observations of intermediate and transitional scale-size equatorial spread F irregularities. Geophys. Res. Lett., 36 (18), L00C05, doi:10.1029/2009GL038905.

Takahashi, H., C. M. Wrasse, C. A. O. B. Figueiredo, D. Barros, M. A. Abdu, Y. Otsuka, K. Shiokawa (2018), Equatorial plasma bubble seeding by MSTIDs in the ionosphere, Prog. Earth Planet. Sci., 5 (32), doi:10.1186/s40645-018-0189-2.

Teillet, P. M., R. P. Gauthier, A. Chichagov (2003), Towards Integrated Earth Sensing: The Role of In Situ Sensing in Real-time, Information Technology for Future Intelligent Earth Observing Satellites, Hierophantes Publishing Services, Pottstown, PA, USA, ISBN: 0-9727940-0-X.

Tulasi Ram, S., P. V. S. Rama Rao, K. Niranjan (2006), The role of post-sunset vertical drifts at the equator in predicting the onset of VHF scintillations during high and low sunspot activity years, Ann. Geophys., 24, 1609–1616, doi:10.5194/angeo-24-1609-2006.

Woods, T. N., A. Caspi, P. Chamberlin, A. Jones, R. Konert, X. Li, S. Palo, S. Solomon (2013), MinXSS - Miniature X-ray Solar Spectrometer (MinXSS) CubeSat Mission, Submitted to NASA, Retrieved from: https://www.pinheadinstitute.org/wp-content/uploads/2014/07/MinXSS_Proposal2013_NASA.pdf.

Woodman, R. F., and C. La Hoz (1976), Radar observations of F regionequatorial irregularities, J. Geophys. Res., 81(31), 5447–5466, doi:10.1029/JA081i031p05447.

Yeh, H. C., S. Y. Su, Y. C. Yeh, J. M. Wu, R. A. Heelis, B. J. Holt (1999), Scientific mission of the IPEI payload onboard ROCSAT-1, Terr. Atmos. Ocean. Sci., 10 (1), 19–42, doi:10.3319/TAO.1999.10.S.19(ROCSAT).

Zhong, P., X. L. Ding, D. W. Zheng, W. Chen, D. F. Huang, (2008), Adaptive wavelet transform based on cross-validation method and its application to GPS multipath mitigation, GPS Solut., 12, 109–117, doi:10.1007/s10291-007-0071-y.

2020 Conference on Weather Analysis and Forecasting
Transfer of Copyright Agreement

The author(s), while submitting the paper, agree(s) that the information and files provided does not infringe any clause of this agreement. This form must be signed and returned before your submission is accepted.

The paper titled:
IDEASSat: A 3U CubeSat mission next on the pad for ionospheric science

I hereby declare, on behalf of myself and my co-authors, that the paper titled above is submitted to 2020 Conference on Weather Analysis and Forecasting, and is authorized to be published in the conference proceedings and on the conference website. I am/we are the sole author(s) of the paper and maintain the authority to enter into this agreement. Moreover, this paper does not contravene any existing copyright or any other third party rights. I will hold the Central Weather Bureau (hereafter, CWB), organizer of this conference, harmless against any suits, proceedings, and claims regarding copyright.

Copyright to this paper (including without limitation, the right to publish the paper in part or in whole, in any and all forms) is hereby transferred to the CWB to ensure widest protection and dissemination against infringement. The CWB proclaims no proprietary right other than copyright. The declaration above is Irrevocable.

Date: 2020.08.28 **Signed:** Duann Yi

First author/Authorized agent for joint authors

Do you agree that your presentation files to be published and shared on the conference website?

- ■ Yes
- ☐ No
- ☐ Otherwise，_____

Signed: Duann Yi